

trometer data using stellar occultations after the 13 December flyby. The chemical composition of the upper atmosphere of Titan along the spacecraft track, derived from mass spectrometer measurements, is reported by Waite *et al.* on page 982 (7).

The desire to understand the formation and evolution of extrasolar planetary systems also motivates the detailed study of the Saturn system. Cassini observations will not only test and validate models of the processes that shaped the saturnian system into its collection of rings, satellites, and plasma; they will also provide an improved theoretical basis for understanding the conditions necessary for the emergence of planetary systems around young stars.

The in situ measurements provided by Cassini's flight through the upper atmosphere of Titan may constrain models of how this moon formed (11). For example, if CO and N<sub>2</sub> were dominant in the formation region of Saturn, clathrates (inclusion compounds within a host lattice such as water) of these molecules, together with the primordial and chemically inert <sup>36</sup>Ar and <sup>38</sup>Ar that were present during Titan's formation,

might be incorporated into the planet. Alternatively, the source of the present N<sub>2</sub> atmosphere might be NH<sub>3</sub> that was later transformed into nitrogen. Measurements of the <sup>36</sup>Ar and <sup>38</sup>Ar argon isotopes relative to the radiogenic <sup>40</sup>Ar (released later into this atmosphere from the decay of <sup>40</sup>K) may distinguish between these alternatives. Likewise, tests of how much of Titan's atmosphere may have been lost over its history can come from measurements of the isotope ratios <sup>15</sup>N/<sup>14</sup>N, because loss to space fractionates these isotopes, with preferential loss of the lighter <sup>14</sup>N. The Cassini Orbiter mass spectrometer data (7), combined with Huygens Probe mass spectrometer (12) measurements of these same isotope ratios in the deep atmosphere, will provide better observational constraints on models of Titan formation.

The Cassini Orbiter/Huygens Probe mission provides an extraordinary example of a successful international collaboration in space exploration. The navigation (9) of this sophisticated science platform precisely to its targeted destination in Titan's upper atmosphere, the successful deployment and entry of the Huygens Probe, the solid performance from the large number of instru-

ments, and the demonstration of the ability to flawlessly plan and execute complex measurement sequences are a tribute to the skill, dedication, and perseverance of the multinational Cassini team. Future Titan flybys will incrementally build up the map of Titan's surface and sample the atmosphere at different locations and seasons. The data from the first flyby reported here (1-7) provide a preview of the insights that can be expected from the next several years of exploration and are the first steps toward a substantially deeper understanding of this distant world.

#### References

1. C. Elachi *et al.*, *Science* **308**, 970 (2005).
  2. F. M. Flasar *et al.*, *Science* **308**, 975 (2005).
  3. H. Backes *et al.*, *Science* **308**, 992 (2005).
  4. D. G. Mitchell *et al.*, *Science* **308**, 989 (2005).
  5. J. E. Wahlund *et al.*, *Science* **308**, 986 (2005).
  6. D. E. Shemansky *et al.*, *Science* **308**, 978 (2005).
  7. J. H. Waite Jr. *et al.*, *Science* **308**, 982 (2005).
  8. M. G. Kivelson *et al.*, *Science* **289**, 1340 (2000).
  9. R. D. Lorenz, J. Mitton, *Lifting Titan's Veil* (Cambridge Univ. Press, Cambridge, UK, 2002).
  10. A. A. Wolf, *Space Sci. Rev.* **104**, 101 (2002).
  11. T. Owen, D. Gautier, *Space Sci. Rev.* **104**, 347 (2002).
  12. H. B. Niemann *et al.*, *Space Sci. Rev.* **104**, 551 (2002).
- 10.1126/science.1113205

#### REPORT

## Cassini Radar Views the Surface of Titan

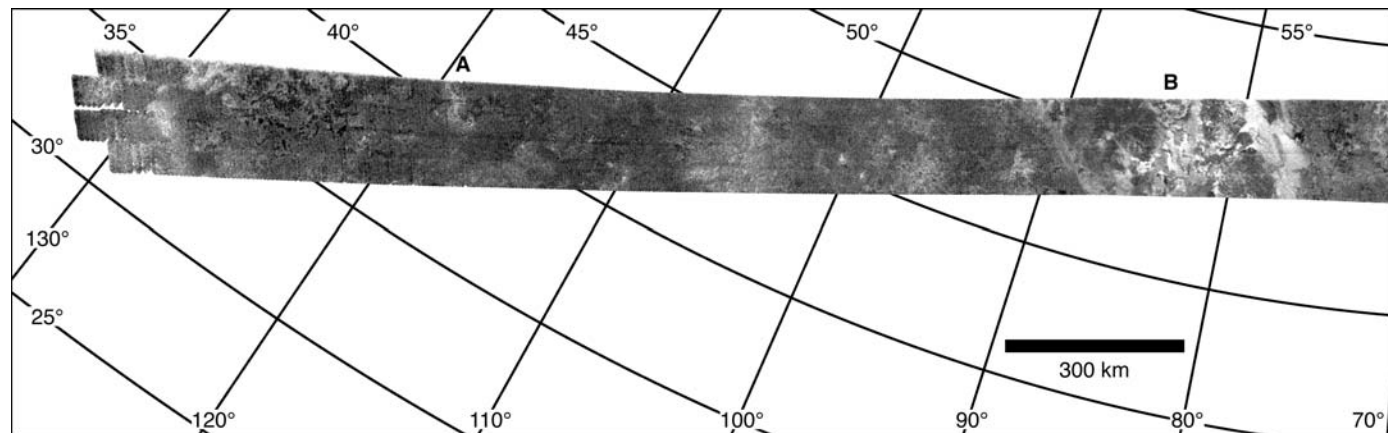
C. Elachi,<sup>1</sup> S. Wall,<sup>1\*</sup> M. Allison,<sup>2</sup> Y. Anderson,<sup>1</sup> R. Boehmer,<sup>1</sup> P. Callahan,<sup>1</sup> P. Encrenaz,<sup>3</sup> E. Flamini,<sup>4</sup> G. Franceschetti,<sup>5</sup> Y. Gim,<sup>1</sup> G. Hamilton,<sup>1</sup> S. Hensley,<sup>1</sup> M. Janssen,<sup>1</sup> W. Johnson,<sup>1</sup> K. Kelleher,<sup>1</sup> R. Kirk,<sup>6</sup> R. Lopes,<sup>1</sup> R. Lorenz,<sup>7</sup> J. Lunine,<sup>7</sup> D. Muhleman,<sup>8</sup> S. Ostro,<sup>1</sup> F. Paganelli,<sup>1</sup> G. Picardi,<sup>9</sup> F. Posa,<sup>10</sup> L. Roth,<sup>1</sup> R. Seu,<sup>9</sup> S. Shaffer,<sup>1</sup> L. Soderblom,<sup>6</sup> B. Stiles,<sup>1</sup> E. Stofan,<sup>11</sup> S. Vetrella,<sup>5</sup> R. West,<sup>1</sup> C. Wood,<sup>12</sup> L. Wye,<sup>13</sup> H. Zebker<sup>13</sup>

The Cassini Titan Radar Mapper imaged about 1% of Titan's surface at a resolution of ~0.5 kilometer, and larger areas of the globe in lower resolution modes. The images reveal a complex surface, with areas of low relief and a variety of geologic features suggestive of dome-like volcanic constructs, flows, and sinuous channels. The surface appears to be young, with few impact craters. Scattering and dielectric properties are consistent with porous ice or organics. Dark patches in the radar images show high brightness temperatures and high emissivity and are consistent with frozen hydrocarbons.

Saturn's largest satellite, Titan, is the only moon and one of only four solid bodies in the solar system to host a thick atmosphere,

uniquely distinguished by nitrogen and methane and a complex suite of organic products of these molecules. Its primitive chemistry

may reveal clues about the prebiotic origin of materials that ultimately gave birth to life in our solar system. The mapping of Titan is an especially challenging puzzle because the most likely constituent materials (e.g., water-ammonia and other ices, hydrocarbons, tholins) in this chemical and temperature regime are likely to exhibit different scattering properties than at Earth and Venus, the only other worlds mapped by spaceborne radar (1-3).



The Cassini mission's Titan Radar Mapper operates in four modes: radiometry, scatterometry, altimetry, and synthetic aperture radar (SAR) imaging (4). SAR mode requires ranges less than  $\sim 4000$  km; high-resolution SAR ( $\sim 500$  m/pixel) can be collected only below  $\sim 1500$  km. Data reported here are from the first close flyby, designated  $T_A$ , which occurred on 26 October 2004 at a minimum range of 1174 km, the first of 45 planned close flybys (4). Inbound full-disk radiometry and scatterometry scans of large regions, including the Huygens probe landing site (5, 6), were acquired from  $\sim 25,000$  km at differing angles. SAR coverage extending through closest approach over an arc of  $\sim 100^\circ$  was followed immediately by an altimetry track covering an arc of  $\sim 10^\circ$ . Scatterometry scans and radiometry scans in orthogonal linear polarizations were collected outbound. Observation geometries and details, coverage diagrams, and higher resolution images are available in (4).

The SAR image strip (Fig. 1; Fig. 2 in detail) reveals a variable surface with distinct units and features. On the basis of brightness, texture, and morphology, we define five units,

two of regional scale and three of local scale. About one-quarter of the swath is composed of a regional-dark, homogeneous unit with relatively low backscatter (see the bottom half of Fig. 2A and parts of Fig. 2, D and E), which includes regions of variable backscatter with indistinct boundaries and scattered SAR-bright spots that may be small topographic features. Most of the rest of the swath consists of a higher backscatter, regional-mottled unit that is gradational at its boundaries with the darker, homogeneous unit. Two discrete SAR-bright units are distinguished. A bright lobate unit (Fig. 2E) occurs in several locations across the swath. The lobate boundaries range from distinct to gradational, with variable brightness across the unit. Both sheet-like and more digitate examples appear, sometimes associated with quasi-circular features. A bright, lineated unit exhibits sharp boundaries and bright, lineated interiors (Fig. 2C). The lineations are parallel and are spaced 1 to 2 km apart. This unit appears similar to grooved terrains seen at several scales on Ganymede (7, 8). The fifth unit is SAR-dark and occurs as isolated patches a few tens of kilometers or less across (Fig. 2, B to D). One such dark patch is near the western end of the swath. These patches tend to be irregular, with sharp boundaries; many are interconnected by narrow sections, giving the impression that their distribution is topographically controlled, perhaps by depressions, valleys, and channels.

A large, roughly circular feature about 180 km in diameter is prominent in the SAR strip, centered near  $50^\circ\text{N}$ ,  $87^\circ\text{W}$  (Fig. 2B, at left). The International Astronomical Union (IAU) has provisionally approved the name Ganesa Macula for this feature. It has suggestions of a volcanic construct, possibly a dome; it could also occupy an old impact scar. Along its edges are SAR-bright flanks; at its center, instead of a central peak, is an apparent central depression, about 20 km in its longest dimen-

sion, that resembles a volcanic crater. Several sinuous channels and/or ridges radiate from the central feature; these appear to carry material from the center. The 90-km sinuous features trending southeast could be responsible for transport of material to the SAR-bright regions along the flank. The terrain along the eastern margin is complex, exhibiting multiple lobate forms that may be flows.

A plot of the scatterometry backscatter cross section versus incidence angle shows both specular and diffuse-scattering echoes (Fig. 3A). The region where specular reflections could be observed was restricted by the Titan-spacecraft geometry to the central part of the inbound scatterometer raster map, but diffuse scattering was observable over a larger area, and the plot indicates considerable heterogeneity. Figure 3B shows a crude classification of the scatterometer measurements into high, medium, and low diffuse cross-section classes, with their locations plotted on Cassini Imaging Science Subsystem (ISS) imagery (9). This model-independent classification shows cross sections clearly correlated with the near-infrared (near-IR) albedo observed by ISS. Figure 4A shows a map of the cross section normalized to constant incidence angle by a simple cosecant model, revealing a strong correlation with the ISS image (Fig. 4C) in the low incidence angle region as well. Xanadu, the bright, continent-sized region at  $90^\circ$  to  $150^\circ\text{W}$ , shows the strongest backscatter, including a particularly bright spot near  $120^\circ\text{W}$  that is undistinguished in the near-IR.

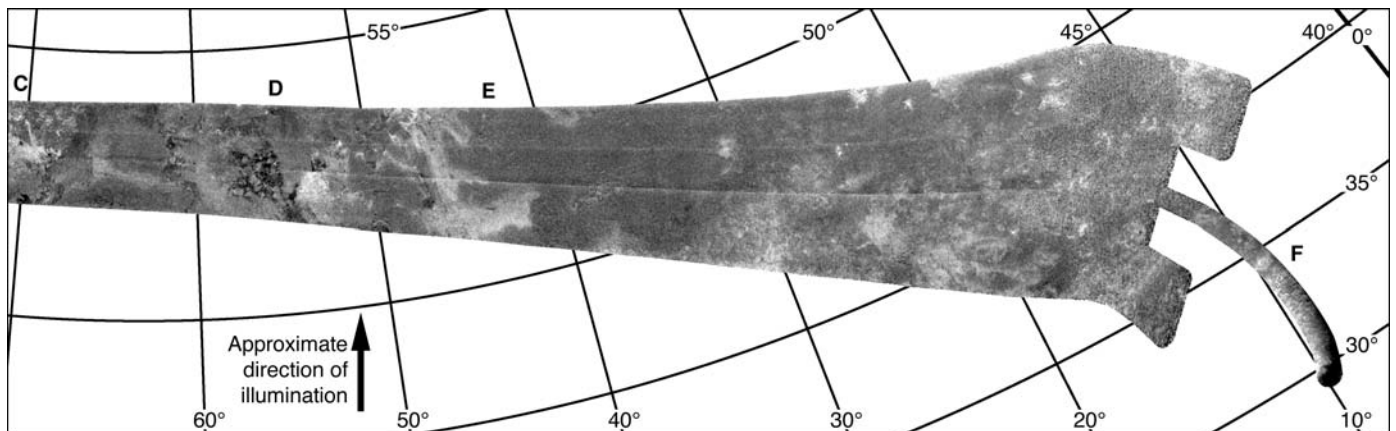
The passive radiometer mode acquired an inbound unresolved disk brightness measurement and two low-resolution outbound microwave brightness maps. Disk-averaged brightness temperatures from these observations are 85 K, 85 K, and 86 K (each  $\pm 5$  K), respectively, consistent with Earth-based measurements (10, 11). Assuming a physical surface temperature of 94 K, these data

<sup>1</sup>Jet Propulsion Laboratory, California Institute of Technology, Pasadena, CA 91109, USA. <sup>2</sup>Goddard Institute for Space Studies, National Aeronautics and Space Administration, New York, NY 10025, USA. <sup>3</sup>Observatoire de Paris, 75014 Paris, France. <sup>4</sup>Agenzia Spaziale Italiana, 00198 Rome, Italy. <sup>5</sup>Facoltà di Ingegneria, 80125 Naples, Italy. <sup>6</sup>U.S. Geological Survey, Flagstaff, AZ 86001, USA. <sup>7</sup>Lunar and Planetary Laboratory, University of Arizona, Tucson, AZ 85721, USA. <sup>8</sup>Division of Geological and Planetary Sciences, California Institute of Technology, Pasadena, CA 91125, USA. <sup>9</sup>Università La Sapienza, 00184 Rome, Italy. <sup>10</sup>INFM and Dipartimento Interateneo di Fisica, Politecnico di Bari, 70126 Bari, Italy. <sup>11</sup>Proxemy Research, Laytonville, MD 20882, USA. <sup>12</sup>Planetary Science Institute, Tucson, AZ 85719, USA. <sup>13</sup>Stanford University, Stanford, CA 94305, USA.

\*To whom correspondence should be addressed. E-mail: steve.wall@jpl.nasa.gov

**Fig. 1** (on facing pages). SAR image strip acquired by Cassini's Titan Radar Mapper during the Titan  $T_A$  flyby, with  $5^\circ$  latitude  $\times$   $10^\circ$  west longitude graticule. Resolution is  $\sim 500$  m at image center, increasing to

$\sim 1400$  m at eastern end. The image has been corrected to constant incidence angle with the use of the backscatter model shown in Fig. 3A and logarithmically scaled. Letters indicate regions enlarged in Fig. 2.



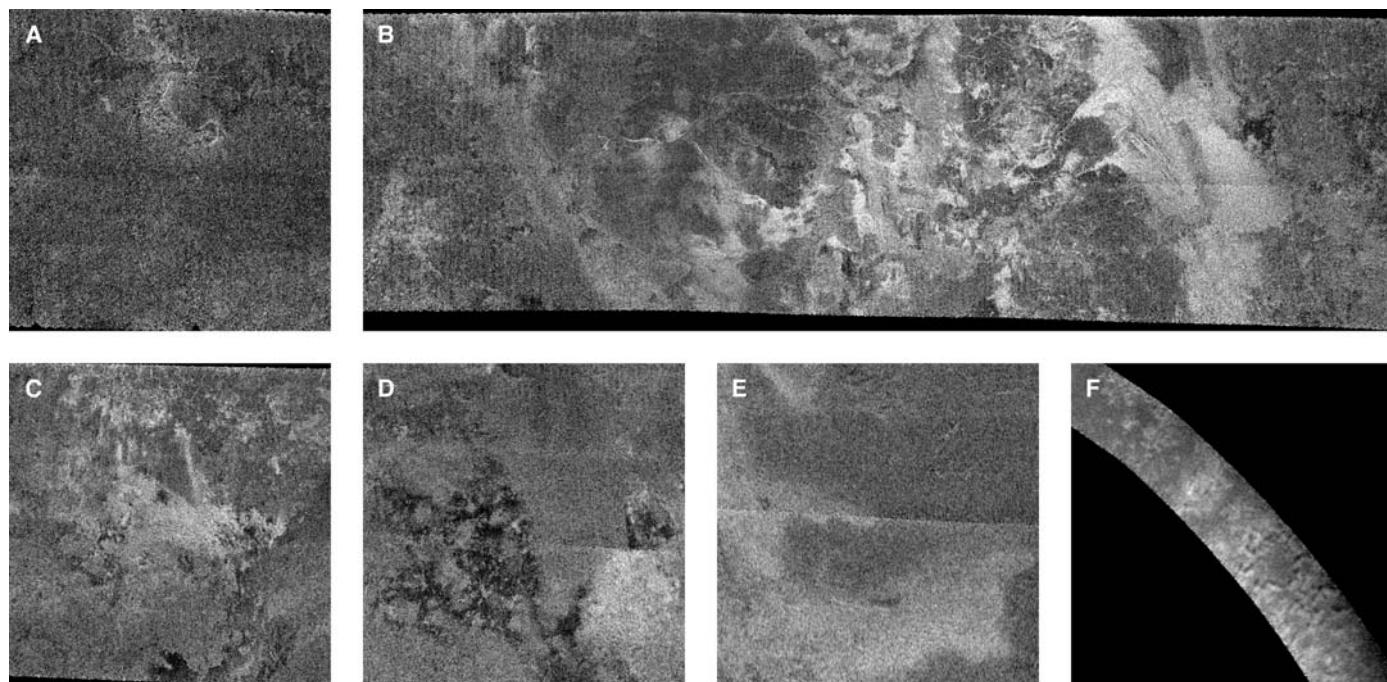


**Fig. 2.** Enlargements of the Cassini SAR image shown in Fig. 1. The letters correspond to the locations shown along the edge of the SAR strip in Fig. 1. Each image covers an area  $\sim 175$  km high, with north approximately at top and illumination approximately from bottom. See text.

correspond to an overall surface emissivity of  $\sim 0.9$ . For a dielectric surface that can be characterized by the Fresnel equations, this is consistent with a dielectric constant of 2 to 3. The polarization and center-to-limb brightness distributions of the full-disk radiometer images are consistent with a uniform surface temperature and a bulk dielectric constant  $\epsilon = 2$ , and are inconsistent with solid water ice ( $\epsilon = 3.1$ ) or ammonia ice ( $\epsilon = 4.5$ ). In particular, the polarization differences yield broadly uniform solutions for  $\epsilon = 2.1$  and 1.6, respectively, in northern and southern mid-latitude regions. The radiometry maps show considerable brightness temperature variations  $\leq 10$  K between regions  $\leq 500$  km in extent that can be attributed to emissivity variations (Fig. 4B). These variations are negatively correlated with those of the backscatter cross section.

Altimetry data were analyzed by a simple threshold algorithm and reduced to elevations relative to a sphere (Fig. 5); absolute radii are awaiting more accurate trajectory data. Relief along the altimetry track covered in this northern region is quite low, varying only  $\sim 150$  m over 400 km. This is a small sample (0.02% of the surface) and does not currently coincide with SAR or optical coverage. However, Cassini radiometry and scatterometry maps of the outbound hemisphere (4) and ISS images (9) indicate that the altimetry does not cross any notable terrain boundaries. The SAR images also provide information about topographic relief of resolved geologic features, but without the geometric rigor of the altimetry. A few features in the SAR swath exhibit the close bright-dark downrange pairing that is charac-

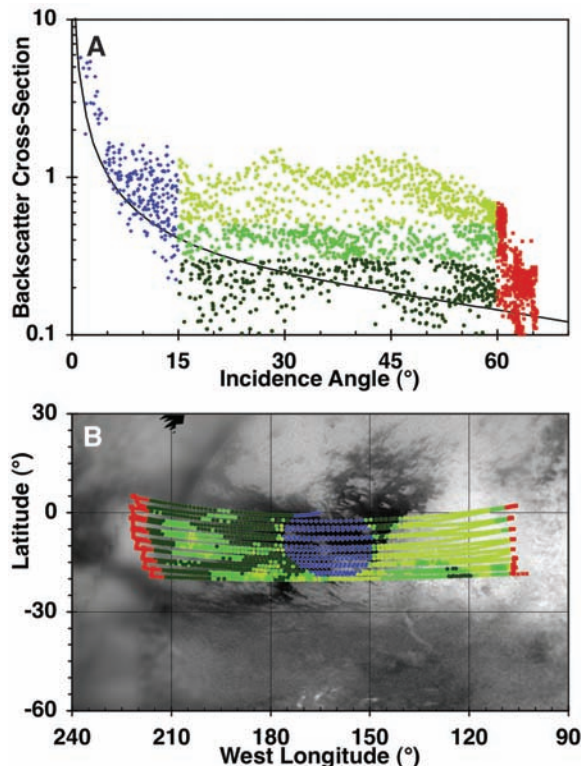


**Fig. 3.** Angular and spatial dependence of Cassini Titan T<sub>1</sub> inbound scatterometer data. (A) Plot of backscatter cross section versus incidence angle shows specular behavior at small incidence angles (blue) and dropoff at largest incidence angles (red). Data at intermediate angles (green) show multiple populations (i.e., surface units) with distinct and only weakly incidence-dependent cross section. Data have been classified into low, medium, and high cross section (dark to light green). Curve is simple cosecant (incidence) backscatter model used to normalize images in Figs. 1 and 2 and scatterometry in Fig. 3A. (B) Map of scatterometer measurements overlaid on Cassini ISS image map (9), colored according to incidence angle and backscatter classification as in (A). High- and low-incidence classes are geographically restricted because of observation geometry, but cross-section classes at intermediate angles correlate clearly with near-IR albedo.

teristic of topographic shading. Radarclinometric analysis allows crude estimates of heights. The strongest sense of relief is given by small apparent hills, 5 to 10 km in width (Fig. 2F). Many of these show bright-dark pairing in the downrange direction, making it unlikely that they are flat surfaces of variable scattering. They were imaged at a lower incidence angle

relative to most of the strip, maximizing topographic modulation. We estimate that the relief is only  $\sim 100$  m and slopes are  $\sim 3^\circ$  to  $5^\circ$  (12). Applying this approach to a flow-like feature at  $41^\circ$ W,  $47^\circ$ N indicates a height of  $\sim 250$  m, bounding slopes of  $\sim 7^\circ$ , and a flat top.

The potential pitfalls of overinterpreting brightness as slopes may be illustrated by the

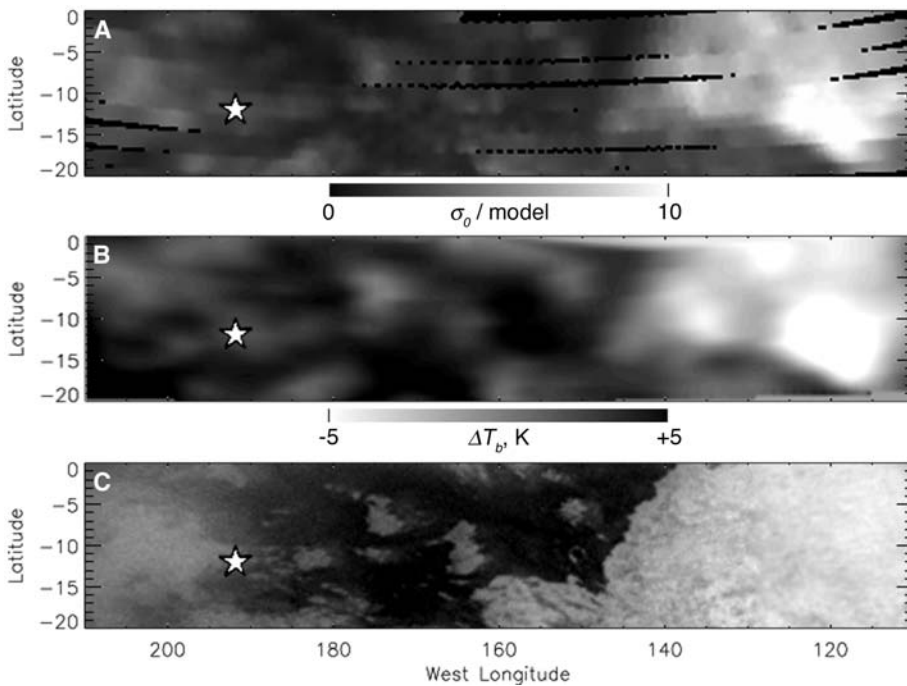
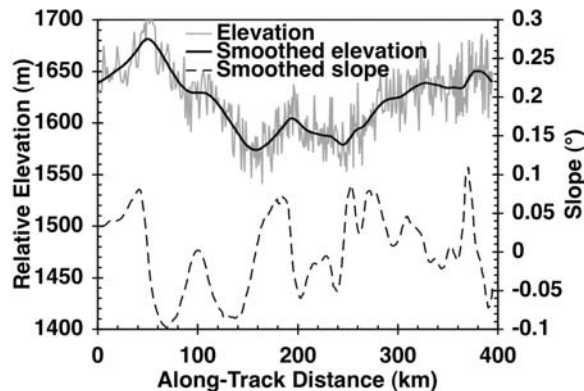


**Fig. 4.** Comparison of radar scatterometry and radiometry with near-IR albedo for a subset of the region in Fig. 3. Simple cylindrical projection is shown, with north at top. Star indicates approximate landing site of Huygens probe. (A) Backscatter cross section  $\sigma_0$  normalized to constant incidence angle according to model curve from Fig. 3A. Black indicates data gaps where scan raster separation exceeded beam width. (B) Deviation of brightness temperature  $T_b$  from model, plotted with reversed grayscale to facilitate comparison. (C) Portion of ISS image mosaic (9). Negative correlation between scatterometry and radiometry is near-perfect, given slightly coarser resolution of latter. Radar-ISS correlation is also strong but has noteworthy exceptions such as extremely radar-bright, low-emissivity spot within Xanadu Regio at 120°W, which is undistinguished optically.

**Fig. 5.** Cassini radar altimetry profile. Leftmost data shown are near 10°W, 29°N, trending south-southeast. Raw elevations relative to a 2575-km sphere (gray) have been smoothed by convolution with a Gaussian function with standard deviation  $\sim 7$  km (solid black line) to suppress the point-to-point variations (root mean square  $\sim 20$  m) due to noise; bi-directional slopes were calculated from the smoothed elevations. Horizontal resolution is limited by beam width to  $\sim 25$  km. Only elevation changes within the profile are significant, given current errors in trajectory information used to reduce the data.



large, bright, flow-like feature shown in Fig. 2E. Backscatter varies linearly across this feature, so if it is topographic, it is roughly parabolic in cross section, with maximum slopes of  $\pm 4^\circ$ ; the height of the 70-km-wide eastern part is  $\sim 1000$  m. These dimensions are comparable to thick flows on Ariel (13) and would require an implausibly large amount of geothermal heat to be expressed over time as cryomagma. An alternative interpretation that we prefer, given the diffuse appearance of the feature, is that brightness is related to a compositional or textural gradient on the surface of a much thinner flow.

Given Titan's unique combination of atmosphere and temperature, the interpretation of these data is necessarily speculative until coverage is increased and is obtained from multiple instruments. Most notable is the lack of unambiguous impact craters visible in the SAR strip. Objects producing craters smaller than  $\sim 20$  km would be screened by Titan's present atmosphere (14, 15). Heavily cratered terrains on other large saturnian satellites typically have 200 to 400 craters per  $10^6$  km<sup>2</sup> larger than  $\sim 20$  km (16); we should expect to find 100 to 200 craters here if this were an ancient surface. With no fresh craters and only

a few degraded candidates, the resurfacing rate must be considerably higher than the impact cratering rate. We conclude, therefore, that this part of Titan's surface is geologically young. Crater obliteration may be due to burial, either by deposition of stratospheric photochemical debris or direct accretion and windblown deposition; pluvial erosion or deposition; tectonic processes; or cryovolcanism. The lobate units, channels, and other flow-like features suggest pluvial or volcanic processes; the presence of apparent volcanic constructs and a simple calculation of available resurfacing materials (17) favor cryovolcanism.

The SAR and scatterometer observations are consistent with previous Earth-based data, even though the wavelengths and the specific areas observed differ. Arecibo (wavelength = 13 cm) observations of Titan show a diffusely scattered component, with a weak specular component present for about 75% of the observation (18), indicating smooth surfaces with slopes as shallow as  $0.2^\circ$  and Fresnel reflectivities of several percent. The specular component has not been seen in radar observations of other icy solar system bodies; it requires the existence of regions that are nearly flat at subcentimeter scales. However, diffuse reflection of most of the echo power requires near-surface structural complexity (e.g., roughness or fractures and voids) at scales  $\geq 0.5$  cm. Surface roughness alone from geochemically plausible minerals would be too weak to produce the observed echoes. Therefore, although surface roughness per se may contribute to variations in the radar brightness, we concur with Campbell and co-workers (18) and attribute the bulk of Titan's radar echo (away from the specular peak in Fig. 3) to volume scattering, in which case multiple scattering in icy materials is known to be able to produce strong returns.

Titan's scatterometry, with both specular and diffuse components, in some ways resembles those of the Moon and the inner planets (19), albeit at a much higher magnitude. Such large variations in radar brightness in both components suggest that Titan's near-surface structure and composition are heterogeneous. Volume scattering depends critically on the transparency of the medium (20, 21) and would be much greater for nearly pure water ice [as on the icy Galilean satellites (22)] than if absorbing material such as ammonia or silicates were present, as may be the case for Iapetus (23) and comets (24). Therefore, variability in composition remains an important candidate to explain variations in radar reflectivity, although we believe volume scattering in low-loss media to be an important effect, particularly in the SAR-bright regions.

At global scale, Titan differs from cold, icy surfaces such as Europa and Ganymede, where microwave emissivities of 0.5 to 0.6 and high radar reflectivity indicate the dominance of

volume scattering from the subsurface rather than from a simple dielectric half space (25). A much more complicated model for Titan, involving multiple surface layers and compositional heterogeneities, may be required to reconcile the Cassini scatterometry and radiometry observations. All materials posed as candidates for Titan's surface other than those containing ammonia are expected to have very low microwave absorption at temperatures  $\sim 100$  K, and would have to be tens of meters deep to produce the observed emission.

The strong correlation between radiometry and optical data (Fig. 4, B and C) is not understood. The strong correlation between the SAR-bright and SAR-dark features and radiometrically cold and warm regions, respectively (Fig. 4, A and B), also suggests that volume scattering is one cause of the SAR-bright regions. If the SAR brightness were solely due to slopes, the correlation with brightness temperature would be positive. Surface roughness alone would have a small effect on thermal emission at the SAR viewing angle. A possible hypothesis is that (i) the optically brighter and colder areas are fractured or porous ice, producing volume scattering and resulting low emissivity, as on the surfaces of Europa and Ganymede; and (ii) the optically darker, warmer, high-emissivity areas have a lower average dielectric constant, being composed of either an organic sludge (26, 27) or a porous material of high dielectric constant, such as water ice.

The location of reservoirs of organic liquid is unclear, although patches of SAR-dark material occupy  $\sim 1\%$  of the swath and may well represent concentrations of organics. So far, these patches have been too small to resolve with radiometry. Shallow deposits of liquid hydrocarbons could, however, be transparent to microwaves, as is the case for cold and pure water ice (28). Alternatively, the liquid hydrocarbons could be masked by floating solids. All materials likely on Titan would sink in liquid ethane and methane, with the exception of the polymerized product of acetylene (polyacetylene), itself the most abun-

dant solid product of stratospheric photolysis (29). Some forms of polyacetylene exhibit microporous structures with density  $\sim 0.4$  g/cm<sup>3</sup>, lower than any expected combination of methane, ethane, and nitrogen in surface liquid form (28, 29). This material is a weak semiconductor and, if suspended or floating on liquids, it could appear relatively bright to radar and optical sensing and would contribute enough small-scale roughness to suppress the specular reflection at optical wavelengths.

From even this limited view of its smallest details, it is clear that Titan's surface is complex and young, although we note again that only 1% of it has been imaged by SAR. As we progress through the mission, we expect SAR coverage of more than 25% of the planet, near-global radiometry and scatterometry coverage, and tens of altimetric profiles, providing increasingly instructive information about the processes at work on Titan.

#### References and Notes

- B. Campbell, *Radar Remote Sensing of Planetary Surfaces* (Cambridge Univ. Press, Cambridge, 2002).
- J. McCauley et al., *Science* **218**, 1004 (1982).
- R. Saunders et al., *J. Geophys. Res.* **97**, 13067 (1992).
- Instrument detail, observation geometries and details, resurfacing rate, radar/radiometry methods, a coverage diagram, and related references are available as supporting material on Science Online.
- The Huygens probe descended on 14 January 2005, reaching the surface at about 10.5°S, 192°W. See (30).
- Titan geographical coordinates are per the IAU (31): In general terms, the equator is roughly Titan's orbital plane, and zero longitude is the subsaturn point, with a libration of  $\pm 3^\circ$  due to orbital eccentricity.
- R. T. Pappalardo et al., in *Jupiter: The Planet, Satellites, and Magnetosphere*, F. Bagenal Ed. (Cambridge Univ. Press, Cambridge, 2004), pp. 363–396.
- J. G. Patel et al., *J. Geophys. Res.* **104**, 24,057 (1999).
- C. C. Porco et al., *Nature* **434**, 159 (2005).
- B. J. Butler, M. Gurwell, *Bull. Am. Astron. Soc.* **36**, 1075 (2004).
- A. Grossman, D. Muhleman, *Bull. Am. Astron. Soc.* **24**, 954 (1992).
- This apparent asymmetry could result from the actual backscatter behavior departing from the assumed  $1/\sin(\theta)$  form at small incidence angles and/or from the finite resolution of the images. Even allowing for these effects, the relief is likely not much more than 100 m, and slopes do not approach the incidence angle, so that the features are not severely distorted by layover.
- D. G. Jankowski, S. W. Squyres, *Science* **244**, 1322 (1988).

- J. Lunine, N. A. Artemieva, R. D. Lorenz, E. Flamini, paper presented at the 36th Annual Lunar and Planetary Science Conference, League City, TX, 14–18 March 2005, abstract 1504.
- S. Engel, J. I. Lunine, W. K. Hartmann, *Planet. Space Sci.* **43**, 1059 (1995).
- R. Lorenz, *Planet. Space Sci.* **45**, 1009 (1997).
- R. Lorenz, *Planet. Space Sci.* **44**, 1021 (1996).
- Campbell et al. (32) conducted observations with the Arecibo and Goldstone radio telescopes in November and December 2001 and late in 2002, obtaining disk-integrated echo spectra at longitudes 23° apart at 26°S.
- S. Ostro, *Rev. Mod. Phys.* **65**, 1235 (1993).
- K. Peters, *Phys. Rev. B* **46**, 801 (1992).
- G. Black, D. Campbell, P. Nicholson, *Icarus* **151**, 167 (2001).
- S. Ostro et al., *J. Geophys. Res.* **97**, 18227 (1992).
- G. J. Black, D. B. Campbell, L. M. Carter, S. J. Ostro, *Science* **304**, 553 (2004).
- J. Harmon, D. Campbell, S. Ostro, M. Nolan, *Planet. Space Sci.* **47**, 1409 (1999).
- D. Muhleman, A. Grossman, B. Butler, *Annu. Rev. Earth Planet. Sci.* **23**, 337 (1995).
- We refer to the complex mix of nitriles and liquid and solid hydrocarbons produced by Titan's atmospheric photochemistry as "sludge." Dielectric constants vary, increasing with increasing mass density, from about 1.6 for methane to 3 or more for higher molecular weight materials, but 2.0 to 2.4 is a representative range for the mix. See (33).
- R. Thompson, *Icarus* **86**, 336 (1990).
- Models for liquid compositions on Titan's surface are discussed in (34).
- The density of polyacetylene is discussed in (35).
- M. Tomasko et al., *Nature*, in press.
- P. K. Seidelmann et al., *Celest. Mech. Dynam. Astron.* **82**, 83 (2002).
- D. B. Campbell, G. J. Black, L. M. Carter, S. J. Ostro, *Science* **302**, 431 (2003).
- R. Lorenz et al., *Planet. Space Sci.* **51**, 353 (2003).
- J. Lunine, *Rev. Geophys.* **31**, 133 (1993).
- D. Bott, in *Handbook of Conducting Polymers*, T. Skotheim, Ed. (Dekker, New York, 1986), pp. 1191–1232.
- We gratefully acknowledge the many years of work by many hundreds of people in the development and design of the Cassini mission that have culminated in the results presented herein. The Cassini Project is a joint endeavor of NASA, the European Space Agency (ESA), and the Italian Space Agency (ASI). Cassini is managed by the Jet Propulsion Laboratory, California Institute of Technology, under a contract with NASA.

#### Supporting Online Material

www.sciencemag.org/cgi/content/full/308/5724/970/DC1

Materials and Methods

Figs. S1 to S4

Table S1

References

18 January 2005; accepted 25 April 2005  
10.1126/science.1109919